Bending Rigidity and Induced Persistence Length of Molecular Bottle Brushes: A Self-Consistent-Field Theory

Laurent Feuz,[†] Frans A. M. Leermakers,[‡] Marcus Textor,[†] and Oleg Borisov*[,§]

Laboratory for Surface Science and Technology, Department of Materials, Swiss Federal Institute of Technology, ETH Hönggerberg, Zürich, Switzerland; Laboratory of Physical Chemistry and Colloid Science, Wageningen University, Dreijenplein, 6, 67003 HB, Wageningen, The Netherlands; and Laboratory of Physical Chemistry of Polymers / UMR 5067, UPPA CNRS, 64053, Pau, France

Received April 23, 2005; Revised Manuscript Received August 11, 2005

ABSTRACT: The two-gradient version of the Scheutjens−Fleer self-consistent-field (SF-SCF) approach is employed for the analysis of the average conformations of side chains and corresponding contribution to the bending rigidity, or equivalently the induced persistence length, of molecular bottle brushes both under good and theta solvent conditions. This study is targeted to unravel conformational properties of poly(L-lysine)-*graft*-poly(ethylene glycol) copolymers in dilute aqueous solutions, where variation of temperature changes the solvent strength for poly(ethylene glycol) in a wide range. We focus on molecular brushes with moderate and high grafting density and large degree of polymerization of grafted chains. In this limit the predictions of an analytical mean-field theory for the dependences of the structural properties of the bottle brush on the architectural parameters are well confirmed. Both the induced persistence length and the ratio between the induced persistence length and the cross-sectional thickness of the bottle brush increase with increasing grafting density and/or increasing degree of polymerization of the grafted chains. However, in the range of moderate chain lengths and grafting densities this ratio remains small, which explains why the effects of the induced bending rigidity on the apparent persistence length have not been observed in earlier numerical experiments. We argue that only molecular bottle brushes with densely grafted long chains possess the potential for lyotropic ordering, both in solutions and at interfaces, due to the expected high effective segment asymmetry.

1. Introduction

Self-assembly of poly(ethylene glycol) (PEG, PEO)-based copolymers at water−solid interfaces is a widely used approach for the modification of surfaces with respect to their biointeractive (protein-resistant) or lubrication properties.[1] The development of protein-resistant surfaces (prevention of nonspecific protein adsorption) is of central interest in the context of the design of biosensor chips and medical implants operating in contact with blood.

An important class of copolymer molecules of special interest is based on a poly(L-lysine) backbone, charged positively due to the presence of protonated amine groups at a neutral pH and grafted with poly(ethylene glycol) side chains (PLL-*g*-PEG).[2] The polyelectrolyte nature of the PLL main chain (backbone) allows the exploitation of the Coulomb attraction as the driving force of self-assembly of PLL-*g*-PEG macromolecules into monolayers at negatively charged metal oxide surfaces.

Conformations of comblike (graft-) copolymers in solutions and their adsorption at interfaces have been extensively studied experimentally,[3−10] theoretically,[11−15] and by means of computer simulations[15−23] over the past decades. The graft-copolymers are classified as molecular bottle brushes when the distance between the grafting points along the contour of the backbone is small in comparison to the characteristic dimensions of the side chains. Scaling theory of conformations of the graft-copolymers in nonselective (good or theta) solvents have been developed in refs 11−15. It was suggested by Birshtein et al.[11] to apply a coarse-grained description of the average conformations of molecular bottle brushes on a large scale. In this approach one assumes that a long graft-copolymer molecule can be envisioned as a wormlike chain with an effective (apparent) contour length, L_{app}, a cross-sectional thickness $2D$ which is determined by the dimensions of the side chains, and the effective (apparent) persistence length, l_{app}. The latter coarse-grained property is determined by the interplay of "bare" stiffness of the backbone and repulsive interactions of grafted chains.

Although it was generally recognized that steric repulsion between side chains reduces the flexibility of the graft-copolymer backbone,[3−8] the contribution of the side chains to the bending rigidity and to the apparent persistence length l_{app} of molecular bottle brushes has been a matter of debate in the literature.

It has been suggested by Fredrickson[14] that repulsions of side chains gives rise to "induced" bending rigidity (or "induced" persistence length) of the molecular bottle brush, i.e., leads to long-range correlations of bending fluctuations on the length scale $\sim l_p$ exceeding by far the characteristic dimensions of the grafted chains. It was pointed out that in the latter case even graft-copolymers with intrinsically flexible backbones possess the property of liquid-crystalline lyotropic ordering in semidilute solutions. However, the scaling approach employed by Fredrickson for the calculation of l_p does not enable one to calculate the absolute value, but rather reveals scaling exponents for l_p as a function of the degree of polymerization of the side chains and the spacers.

[†] Swiss Federal Institute of Technology.
[‡] Wageningen University.
[§] UPPA CNRS.
* To whom correspondence should be addressed: e-mail oleg.borisov@univ-pau.fr; Tel +33-559-40-75-91; Fax +33-559 40 76 23.

10.1021/ma050871z CCC: $30.25
Published on Web 09/17/2005

In contrast, Birshtein et al.[11] have suggested that the rigidity "induced" by the interaction of the side chains (and l_p) is small due to repartitioning of grafted chains from the concave to the convex side of a bent bottle brush. Similar behavior was demonstrated in model calculations for planar polymer brushes.[24] This implies that in molecular bottle brushes with intrinsically flexible backbone the segments of the backbone with the size $\sim D$ keep stretched (extended proportionally to the contour length) conformation, whereas on the length scale larger than D it is randomly coiled. Hence, the bottle brush retains its local cylindrical symmetry only on the length scale of the order of D. Then, the solution of the molecular bottle brushes possesses no ability to lyotropic order even at high concentrations. Moreover, for two-dimensional bottle brushes Monte Carlo (MC) simulations[21,22] and mean-field analytical calculations[25] indicate that excluded-volume repulsions of the side chains may even induce spontaneous curvature which leads to helical in-plane conformations of bottle brushes with flexible backbones.

Finally, MC simulations of Saariaho et al.[18−20] have demonstrated that, upon an increase in the degree of polymerization of the side chains, the apparent persistence length of a 3-dimensional bottle brush with a flexible backbone only grows proportionally to the thickness of the bottle brush, showing that the effective asymmetry of the segment (the ratio between the apparent persistence length and the thickness of the bottle brush) does not increase as a function of, e.g., side chain length.

The aim of the present paper is to apply the powerful numerical self-consistent-field (SCF) computational approach and in particular the method of Scheutjens and Fleer (SF-SCF) for the analysis of structural and mechanical properties of molecular bottle brushes, in particular, those of PLL-*g*-PEG copolymers in water. The benefit of the SCF method over the MC simulations is its very high computational efficiency combined with practically the same accuracy. Moreover, within the SF-SCF method, the mechanical properties of the bottle brush, such as bending modulus, can be directly computed from the partition function, whereas they are only indirectly accessible in MC simulations from the analysis of the shape of the molecular bottle brushes. As a result, using the SF-SCF method, we can examine bottle brushes with a high density of long side chains (high grafting density) and significantly go beyond the limits of MC or molecular dynamics (MD) simulations.

2. Results of Analytical Mean-Field Theory

2.1. Conformations of Polymer Chains in a Bottle Brush. We start with a brief review of the results of analytical theory describing conformations of polymer chains in a cylindrical (bottle) brush, that is, an array of flexible polymer chains with degree of polymerization $n \gg 1$, end-grafted onto a thin long cylinder (a backbone) with a grafting density h^{-1}. The crowding of neighboring chains along the cylinder (chain overlap) is significant when the distance between the grafted chains, h, is much smaller than the characteristic chain dimension along the backbone, i.e., $h \leq n^{1/2}a$ (cf. Figure 1). The grafted chains are assumed to be intrinsically flexible; i.e., the Kuhn segment length is of the order of the monomer size, a.

On the contrary, for the main chain of the graft-copolymer we consider both possibilities, to be semiflexible (stiff) or flexible. An isotropic wormlike chain in 3-dimensional space is characterized by a single bending modulus κ, which is directly related to the persistence length $l = \kappa/k_BT$. The persistence length characterizes the length scale beyond which the chain is randomly bent (coiled) by thermal fluctuations.

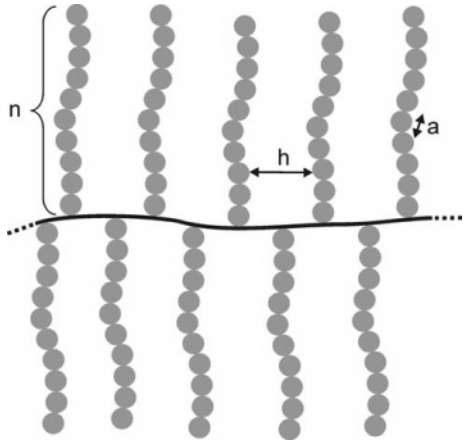

Figure 1. Parameters defining the local architecture of a molecular bottle brush: h = extension of backbone spacers; n = number of monomers in grafted side chain; a = size of a monomer.

The "bare" stiffness (and the "bare" persistence length, l_{bare}) of the backbone may arise due to intrinsic (structural) stiffness, which can be additionally enhanced by long-range Coulomb repulsive interactions of charged monomers of the backbone, as is the case for ionic/nonionic graft-copolymers like PLL-*g*-PEG. In the latter case, the bare rigidity of the backbone can be tuned by variation in pH and/or salinity of the solution. In the case of intrinsically stiff and/or strongly charged polyelectrolytes, the electrostatic contribution to the bare rigidity of the backbone is given by

$$\kappa_{OSF}/k_BT \cong l_B\tau^2 r_D^{\,2} \qquad (1)$$

where OSF refers to the pioneers in this field, Odijk, Skolnik, and Fixman,[26,27] r_D is the Debye screening length, $l_B \cong e^2/\epsilon k_BT$ is the Bjerrum length, and τ is the linear charge density on the main chain measured in number of elementary charges per unit length. Remarkably, the electrostatic repulsion of charged monomers induces stiffening of the main chain on the length scale $\sim l_{OSF} = \kappa_{OSF}/k_BT$, exceeding the characteristic range $\sim r_D$ of the electrostatic interactions. Hence, by an increase in the ionic strength of the solution (leading to a decrease in r_D) or by varying pH (leading to the change in the fraction of charged monomers in the main chain), one can alter the flexibility of the main chain of the PLL-*g*-PEG copolymers over a wide range. In particular, the copolymers can be transformed from a molecular bottle brush with a rigid backbone into one with a flexible backbone.

We start our discussion with the case of a stiff, $l_{bare} \gg h$, backbone. In this case the segments of the main chain separating neighboring grafting points exhibit straight conformations. The bending of the main chain due to thermal fluctuations occurs on distances comprising multiple grafts. This situation is directly addressed in our numerical SCF modeling, where a homogeneous curvature with a radius $R \gg h$ is imposed on the backbone in order to calculate the bending rigidity of the bottle brush induced by interactions of

side chains. Effects arising in the case of flexible, $l_{bare} \leq h$, backbones will be discussed at the end of this section.

The structure of a polymer brush of any morphology is characterized by stretching of the grafted chains in the direction perpendicular to the grafting surface. This extension of individual chains is nonuniform and the chain end position is subjected to strong fluctuations. In planar polymer brushes these fluctuations extend over the whole brush thickness and lead to monotonically decreasing (parabolic under good solvent conditions) polymer density profiles.[28]

In contrast, in the case of cylindrical (as well as spherical) polymer brushes a "dead zone", where no chain ends are present, appears.[29] This dead zone is located deeply inside the brush, i.e., near the grafting points. The appearance of a region free of chain ends is the reason why (in contrast to planar brushes) the asymptotic analytical self-consistent-field solution is not available for the cylindrical (as well as for spherical) brush.

As an alternative, the Flory-type or the scaling approach can be applied, which provides power-law dependences of the main structural and thermodynamic properties of the brush as a function of architectural parameters (h, n) and external conditions. This method leaves the numerical factors and nonpower dependences undefined. As our aim is to compare the exact (within the mean-field approximation) results of the numerical SF-SCF approach to the analytical theory predictions, we present below the mean-field version of the theory.[30]

Within the mean-field approximation the free energy of repulsive monomer−monomer interactions per unit volume in the brush can be presented as a function of local (number) density of monomers $c(\rho)$ at distance ρ from the axis of the brush as

$$\frac{f\{c(\rho)\}}{k_BT} = va^3c^2(\rho) + wa^6c^3(\rho) \qquad (2)$$

where v and w are dimensionless second and third virial coefficients of monomer−monomer interactions, respectively. The second virial coefficient (the monomer excluded-volume parameter) is related to the Flory−Huggins $\chi(T)$ parameter via $v = 0.5 - \chi(T)$ and vanishes under theta solvent conditions, $v(T=\Theta) = 0$. For PEG, like for most of nonionic, water-soluble polymers, the quality of water as a solvent decreases (i.e., $\chi(T)$ increases) upon increasing temperature. At room temperature water is a good solvent for the PEG grafted chains, while an increase in temperature decreases the quality of water as a solvent for PEG, thus approaching theta solvent conditions at about 100 °C. The third virial coefficient is fairly independent of T and is of the order of unity, $w \sim 1$.

Within a Flory-type approach one can obtain the average thickness of the brush $D(h)$ and the free energy per chain in the brush $F(h)$ by balancing the free energy of repulsive interactions per chain with the contribution, $F_{conf}(D(h))/k_BT \cong D^2(h)/n$, that arises due to the conformational entropy penalty resulting from chain extension. The corresponding result is

$$D(h) \cong \begin{cases} n^{3/4}v^{1/4}h^{-1/4}a^{5/4} \\ n^{2/3}h^{-1/3}a^{4/3} \end{cases} \qquad (3)$$

$$F(h)/k_BT \cong \begin{cases} (nv/h)^{1/2}a^{1/2} \\ (n/h^2)^{1/3}a^{2/3} \end{cases} \qquad (4)$$

with the first and second lines referring to the cases of good and theta solvents ($v = 0$), respectively.

The single-exponent (power law) radial decay of the monomer concentration, $c(\rho)$, with a cutoff at $\rho \cong D(h)$ is given by

$$c(\rho) \cong \begin{cases} v^{-1/3}(h\rho)^{-2/3}a^{-5/3} \\ (h\rho)^{-1/2}a^{-2} \end{cases} \qquad (5)$$

The omitted (that is reflected by the sign " $\cong$ ") numerical prefactors in eqs 3−5 are of the order of unity. As follows from eq 3, grafted chains are strongly stretched, $D(h) \gg n^{1/2}a$, provided $h \ll n^{1/2}a$.

We remind the reader that the Flory-type approach described above captures the most essential features of the bottle-brush structure (e.g., eqs 4 and 3 for the free energy and the thickness of the brush are asymptotically exact with the accuracy of numerical factors of the order of unity) but is based on rather severe approximations. In particular, it assumes equal and strong, $D(h) \gg n^{1/2}a$, stretching of the chains in the brush with respect to the Gaussian dimensions. The equal stretching assumption implies that all the free ends of grafted chains are localized at the edge of the bottle brush within a thin cylindrical shell at $\rho \approx D$; i.e., the fluctuations in the radial positions of the free chain ends are neglected. Expressions 3−5 can be derived also using local force balance (or Daoud−Cotton type[31]) arguments, i.e., considering any thin cylindrical shell within a bottle brush as a quasi-planar polymer brush.[32]

In the case of the stiff backbone the average axial distance, h, between the side chains coincides with the distance between the grafting points along the contour of the main chain. In the opposite case of a flexible backbone, the "bare" persistence length of the backbone is of the order of the monomer size, $l_{bare} \sim a \leq h$. Each spacer is a (semi-)flexible chain, which is stretched (partially or completely) to such an extent that the elastic tension built up in the spacers counterbalances the axial stress induced by the repulsions of the side chains. Equations 3−5 remain valid, but h is a function of both the number of monomers in a spacer and the number of monomers in a grafted chain. Under the condition $h \leq n^{1/2}a$ the local cylindrical symmetry of the molecular bottle brush on the length scale equal to or larger than the brush thickness, D, is ensured by the combined effects of the bare rigidity of the backbone and repulsive interactions of grafted chains. When the repulsion of the side chains is not strong enough to induce complete stretching of the spacers, the spacers retain their random coil conformation on a local scale. In this case the extended spacers can be presented as strings of so-called Pincus blobs[33] (see refs 11−13 for details).

2.2. Large-Scale Conformation and Coarse-Graining Approach. As has been discussed above, a sufficiently long graft-copolymer molecule can be envisioned as a wormlike chain with an apparent (effective) contour length, L_{app}, effective thickness $2D$, and an apparent (effective) persistence length, l_{app}. These coarse-grained structural characteristics determine the large-scale conformational properties of the graft-copolymer

chain such as the mean-square gyration radius or the end-to-end distance for the main chain.

The apparent contour length, L_{app}, of the effective wormlike chain coincides with the contour length, L_{con}, of the main chain of the graft-copolymer in the case where the main chain is sufficiently stiff, i.e., the "bare" persistence length of the main chain, $l_{bare} \geq h$. In the opposite case of a flexible, $l_{bare} \ll h$, backbone the apparent contour length L_{app} is smaller than L_{con} due to local flexibility of the spacers.

The thickness, $2D$, of the effective wormlike chain determines the lower cutoff limit for the coarse-grained model. It is equal (with the accuracy of a numerical prefactor of the order of unity) to the characteristic dimensions of the grafted chains in the direction perpendicular to the axis of the bottle brush. When, as a result of thermal fluctuations, two segments of the molecular brush that are separated by a large distance along the backbone approach each other, a large crowding free energy penalty must be paid. This free energy of overlapping of grafted chains makes the segments of the copolymer chain effectively impenetrable over the distance $\sim D$. A similar free energy penalty arises upon bending of the brush with a radius of curvature $R < D$.

The interaction between the grafted chains affects the conformation of the main chain of the bottle brush similar to an effective long-range repulsion between the main-chain monomers. The characteristic range of this repulsion is of the order of the side-chain dimensions.

The bending of the bottle brush with respect to a straight configuration necessarily leads to extra crowding of grafted chains on the concave side; it enhances the repulsive osmotic interactions and leads to further conformational entropy losses. The free energy penalty for the bending of the bottle brush with a curvature radius $R \gg D$ gives rise to the "induced" bending rigidity or induced persistence length of the bottle brush. Because of symmetry reasons, the increase in the free energy (per unit length of the bottle brush) upon bending with a curvature radius $R \gg D$ can be presented as

$$\Delta F(h,R)/h = \frac{\kappa_p}{2R^2} + ... \qquad (6)$$

where "..." corresponds to (neglected) terms of higher order in curvature and κ_p is the induced bending rigidity modulus. The bending of the bottle brush leads to its local compression on the concave side complemented by local extension on the convex side. Applying the general relation[34] $\kappa_p \cong D^2 h(\partial^2 F(h)/\partial h^2)$ between bending and longitudinal extension/compression moduli, one can derive a simple scaling form for the induced bending rigidity modulus for the cylindrical brush of thickness D:

$$\kappa_p \cong F(h)D^2(h)/h \cong k_B T \begin{cases} n^2 v a^3/h^2 \\ n^{5/3} a^{10/3}/h^{7/3} \end{cases} \qquad (7)$$

where $F(h)$ and $D(h)$ refer to the unperturbed (straight) configuration and are given by eqs 3 and 4. The numerical factor omitted in eq 7 depends on the internal structure of the bottle brush and also on its rearrangement (repartitioning of chains from the concave to the convex side) upon bending. The corresponding contribution to the persistence length of the molecular bottle brush is given by

$$l_p = \kappa_p/k_B T \qquad (8)$$

Note that the induced persistence length is defined as a local characteristic of the copolymer chain flexibility only on the length scale larger than the effective repulsion range $\sim D$. Comparing eqs 7 and 8 to eq 3, we find that in scaling terms (neglecting prefactors) $l_p \gg D$ provided that the grafted chains in the bottle brush strongly overlap, $h \ll n^{1/2}a$. However, as follows from the results of our subsequent analysis, the numerical factors in eq 7, which remains undefined within the scaling approach, are significantly smaller than unity.

In the case that the backbone is sufficiently stiff, i.e., $l_{bare} \gg h$, the contribution to the bending rigidity induced by interactions of grafted chains, κ_p, is added to the bare rigidity, κ_{bare}, of the backbone, and the apparent persistence length (manifested in the large-scale conformational properties) is given in this case by

$$l_{app} = \frac{\kappa_p + \kappa_{bare}}{k_B T} = l_p + l_{bare} \qquad (9)$$

The intrinsic stiffness of the backbone together with repulsions between the grafted chains results in a straight configuration of the backbone and cylindrical symmetry of the bottle brush on the length scale of the order of $l_{app} = l_{bare} + l_p \gg D$, beyond which the bottle brush is randomly bent by thermal fluctuations.

Even if the effect of an induced rigidity on the chain conformation is negligible at relatively small values of n (dominance of the bare rigidity), it may become progressively more important upon an increase in n. Moreover, as follows from eqs 3 and 7, κ_p (and l_p) increase faster upon an increase in n than the brush thickness D. Consequently, the total rigidity of the bottle brush is determined by the rigidity of the backbone, $l_{app} \approx l_{bare}$, at small n, while at large n the total rigidity is dominated by the contribution from the grafted chains, $l_{app} \approx l_p \gg l_{bare}$.

In the case of an intrinsically flexible (or semiflexible) backbone, $l_{bare} \leq h$, the main chain gets stretched (up to the size proportional to the number of monomers in the corresponding main-chain segment) due to repulsion of the side chains on the length scale of the order of D, whereas on a smaller length scale $\sim \leq h$ the main chain can retain its flexibility and remain subjected to local bending fluctuations. As a consequence, even molecular bottle brushes with an intrinsically flexible backbone retain a local cylindrical symmetry on the length scale $\geq D$. The apparent (effective) persistence length, which determines the large-scale conformation of the macromolecule, scales as $l_{app} \sim \max\{l_p, \sim D\}$. Hence, in the case of relatively small n, the apparent persistence length scales as the bottle-brush thickness, $l_{app} \sim D$, and no extra stiffening results on a coarse-grained level. Because the ratio l_p/D is an increasing function of n, the effect of the induced rigidity of the molecular bottle brush becomes important, $l_{app} \approx l_p \gg D$, only for sufficiently large n. In the latter case a coarse-grained model of a semiflexible wormlike chain with $l_{app} \sim l_p$ applies.

3. Calculation Method (SF-SCF Approach)

3.1. General Formalism. As outlined in the preceding section, the Scheutjens−Fleer self-consistent-field (SF-SCF) approach assumes that the chains are flexible and composed of spherically symmetric segments with

characteristic length a. The segments fit on a lattice with corresponding characteristic dimension a. This length is used to make the concentrations dimensionless; i.e., we will work with volume fractions $\varphi \equiv ca^3$. The target of the SCF calculations is to deduce the optimal volume fraction profiles that minimize the free energy of the system under the constraint that the system is incompressible, i.e., $\varphi_S(\mathbf{r}) + \varphi(\mathbf{r}) = 1$, where φ_S is the volume fraction of a monomeric solvent and $\mathbf{r}$ is a coordinate referring to a set of $L(\mathbf{r})$ lattice sites within which a mean-field averaging is applied. As we will discuss below, this averaging procedure depends on the specific lattice geometry used. We will first outline the generic features of the SF-SCF method for end-grafted chains before we present the lattice geometry details.

Here we will concentrate on the side-chain properties of the bottle-brush molecules. The arms have segments with ranking number $s = 1, ..., n$. As the first segment of these arms is grafted to the line at coordinate $\mathbf{r}^*$, the inversion symmetry is broken; i.e., the distribution of the end-segment $s = n$ is obviously different from the grafting segment $s = 1$. This is reflected in the way the volume fraction profiles $\varphi(\mathbf{r})$ are computed. The volume fractions of segment s at coordinate $\mathbf{r}_s$ are calculated on the basis of the composition law with the constraint that the first segment is grafted. This is done within a Markov approximation, which ensures that neighboring segments along the chain occupy neighboring lattice sites, but ignoring positional correlations of segments that are not neighbors (freely jointed chain). Keeping in mind that the first segment of the chain is at position $\mathbf{r}_1 = \mathbf{r}^*$, we write the composition law as

$$\varphi(\mathbf{r}_s,s|\mathbf{r}_1,1) = \frac{C}{G(N|\mathbf{r}_1,1)} \frac{G(\mathbf{r}_s,s|\mathbf{r}_1,1)G(\mathbf{r}_s,s|N)}{G(\mathbf{r}_s,s)} \qquad (10)$$

where the geometry-dependent normalization C is chosen such that the grafting density h^{-1} is obeyed. In this equation we introduced (i) the two-point Green's function $G(\mathbf{r}_k,k|\mathbf{r}_l,l)$ which gives the combined statistical weight of all possible walks from segment $s = k$ at coordinate $\mathbf{r} = \mathbf{r}_k$ to $s = l$ at coordinate $\mathbf{r} = \mathbf{r}_l$, (ii) the Green function integrated over one "starting" coordinate, i.e., $G(\mathbf{r}_k,k|l) = \sum_{\mathbf{r}_l} L(\mathbf{r}_l)G(\mathbf{r}_k,k|\mathbf{r}_l,l)$, (iii) the single chain partition function $G(N|\mathbf{r}_1,1) = \sum_{\mathbf{r}_N} L(\mathbf{r}_N)G(\mathbf{r}_N,N|\mathbf{r}_1,1)$, and the free segment distribution function $G(\mathbf{r}_s,s) = G(\mathbf{r}_s,s|\mathbf{r}_s,s)$. The latter quantity is simply given by the Boltzmann law $G(\mathbf{r}) = \exp -u(\mathbf{r})/k_BT$ featuring the self-consistent segment potential $u(\mathbf{r})$:

$$\frac{u(\mathbf{r})}{k_BT} = -\ln(1 - \varphi(\mathbf{r})) - 2\chi\langle\varphi(\mathbf{r})\rangle \qquad (11)$$

where we have made use of the incompressibility constraint $\varphi_S(\mathbf{r}) = 1 - \varphi(\mathbf{r})$. The overall volume fraction of polymer units is given by $\varphi(\mathbf{r}) = \sum_s \varphi(\mathbf{r}_s,s|\mathbf{r}_1,1)\delta(\mathbf{r}_s - \mathbf{r})$ where we have dropped for convenience the information that the first segment is pinned on the line. The angular brackets in eq 11 refer to a local site average, which is lattice-type dependent. The Green functions obey the Edwards diffusion equation, which on a lattice transforms in a set of propagator equations:

$$G(\mathbf{r}_s,s|\mathbf{r}_1,1) = G(\mathbf{r}_s,s)\langle G(\mathbf{r}_{s-1},s-1|\mathbf{r}_1,1)\rangle \qquad (12)$$

$$G(\mathbf{r}_s,s|N) = G(\mathbf{r}_s,s)\langle G(\mathbf{r}_{s+1},s+1|N)\rangle \qquad (13)$$

where the angular brackets again depend on the lattice geometry. These recurrence relations are started by $G(\mathbf{r}_1,1|\mathbf{r}_1,1) = G(\mathbf{r}_1)\delta(\mathbf{r}_1 - \mathbf{r}^*)$ and $G(\mathbf{r}_N,N|N) = G(\mathbf{r}_N)$.

The set of equations is closed and is routinely solved numerically for a self-consistent solution, i.e., for the fixed point where the volume fractions that are used to compute the segment potentials are reproduced by the composition law, up to high precision (at least 7 significant units). In such a self-consistent solution the free energy of the system is computed by $F = \sum_{\mathbf{r}} L(\mathbf{r})f(\mathbf{r})$, where the free energy density $f(\mathbf{r})$ is given by

$$f(\mathbf{r}) = \frac{\varphi(\mathbf{r})}{n} \ln\left(\frac{Cn}{G(N|\mathbf{r}_1,1)}\right) + \ln(1 - \varphi(\mathbf{r})) + \varphi(\mathbf{r})\chi\langle\varphi(\mathbf{r})\rangle \qquad (14)$$

3.2. Implementation Issues. For infinitely long bottle brushes in the straight-backbone configuration we may ignore the end effects. In this case we are interested in the free energy per unit length, and the problem can be solved in a one-gradient cylindrical coordinate system. The normalization constant of eq 10 is given by $C = a/h$, where a equals 0.5 nm. In this case $\mathbf{r}$ is replaced by the radial coordinate $r = 1, ..., r_M$, where $r = 1$ is the central lattice layer (where the first segment is grafted, i.e., $r^* = 1$) and $r = r_M$ is a lattice layer sufficiently far from the backbone where bulk solvent is present, i.e., $\varphi_S(r_M)$. In the cylindrical coordinate system the number of sites per unit length is simply $L(r) = \pi(2r - 1)$. The site averages, expressed above by the angular brackets, are given by

$$\langle X(r)\rangle = \lambda_{-1}(r)X(r-1) + \lambda_0(r)X(r) + \lambda_1(r)X(r+1) \qquad (15)$$

It is possible to show that $\langle X(r)\rangle \approx X(r) + {}^1/_6\nabla X(r)$ (assuming $X(r)$ is continuous). The transition probabilities obey the internal balance equation $L(r)\lambda_1(r) = L(r+1)\lambda_{-1}(r+1)$. The contact area between the lattice layers r and $r+1$ is given by $A(r) = 2\pi r$. Using this area, we write for a simple cubic lattice

$$\lambda_1(r) = \frac{1}{6}\frac{A(r)}{L(r)}; \quad \lambda_{-1}(r) = \frac{1}{6}\frac{A(r-1)}{L(r)} \qquad (16)$$

and the remaining transition probability follows automatically from $\lambda_0(r) = 1 - \lambda_1(r) - \lambda_{-1}(r) = \lambda_0 = 4/6$.

The bending rigidity of the molecular bottle brush is probed by imposing a homogeneous curvature to the backbone. This system requires the development of an advanced SCF formalism that keeps track of two gradients in a self-consistent field.

In the two-gradient SCF system, the parameter $\mathbf{r}$ is substituted by a pair of coordinates (z,r) where $z = 1, ..., z_M$ is the coordinate along the axes of the cylindrical coordinate system and $r = 1, ..., r_M$ is the radial direction as used above (Figure 2). The number of sites in each coordinate is computed by $L(z,r) = L(r) = \pi(2r - 1)$. The chains are grafted at some coordinate $\mathbf{r}^* = (z^*,r^*)$, and we consider a perfect ring-shaped molecule with an imposed curvature given by $J = 1/r^*$. The normalization constant of eq 10 is $C = L(r^*)a/h$. This results in nine transition probabilities that are given by $\lambda_{i,j}(r)$, where $i = -1, 0, 1$ for steps in the z-direction and $j = -1, 0, 1$

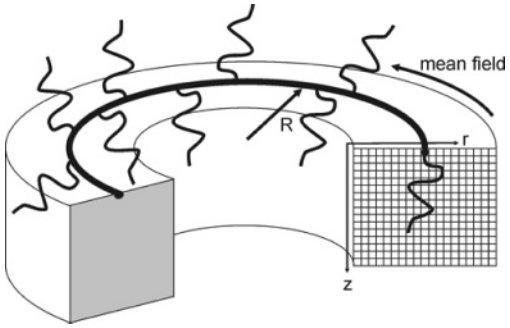

Figure 2. Two-gradient cylindrical lattice system used for the SCF calculations. Mean field is applied along the backbone which gets bent into a torus (only part of the torus shown for clarity reasons).

for those in the r-direction, and the site fraction is found to be

$$\langle X(z,r)\rangle = \sum_{i=-1,0,1}\sum_{j=-1,0,1} \lambda_{i,j}(r)X(z+i,r+j) \quad (17)$$

Next, it is assumed that the steps in the z and r directions are independent and $\lambda_{i,j}(r) = \lambda_i\lambda_j(r)$, where the a priori transition probabilities in the z-direction are given by the flat lattice values $\lambda_{-1} = \lambda_1 = {}^1/_6$ and those in the radial direction are given by eq 16.

The model of end-grafted chains in the one-gradient cylindrical lattice is not exactly identical to the two-gradient result for the radius $r^* \to \infty$. This is because in the one-gradient system the number of sites per unit length in coordinate $r = 1$ equals $L(1) = \pi$ and not unity. However, the noncurved limit is exactly recovered in the two-gradient flat lattice. In this case $\mathbf{r}$ is given by the pair of coordinates (z,x), where the mean-field averaging is done in the y-direction. The step probabilities are $\lambda_{i,j} = \lambda_i\lambda_j$, where in both directions the transition probabilities are given by the flat lattice values. This results in $L(z,x) = 1\ \forall z,x$ and the normalization constant $C = a/h$.

Although the two-gradient SF-SCF calculations are efficient in CPU time, the memory usage may become limiting, e.g., for very large arms. To optimize the range of molecular weights that can be considered, in the case of a bottle brush in solution one may make use of the symmetry of the problem. As the reflecting (Neuman) boundary conditions on all system boundaries are implemented, one can pin the arms of the bottle brush to the coordinate $\mathbf{r}^* = (1,r^*)$ and consider only one-half of the bottle brush to be in the system; the mirror image corresponds then to the other side of the system boundary. In this way one can accommodate longer chain $M_z \times M_r$ systems compared to the situation of chains pinned in the center of the coordinate system, e.g., at $\mathbf{r}^* = (M_z^*/2,r^*)$.

Below we will also examine the bottle brush adsorbed onto a solid substrate. In this case the absorbing boundary condition is imposed at one of the (flat) interfaces.

Obviously, it is possible to minimize the computation time by disregarding all lattice coordinates where the bottle-brush segments cannot possibly enter. This is used to model weakly curved bottle brushes, i.e., for large values of r^*.

4. Results of the SCF Calculations

4.1. Conformations of Grafted Chains. We start with the description of conformations of grafted chains in a bottle brush with a straight or weakly bent configuration of the backbone for which the conformational structure of the brush remains virtually unaffected by the small curvature of the backbone.

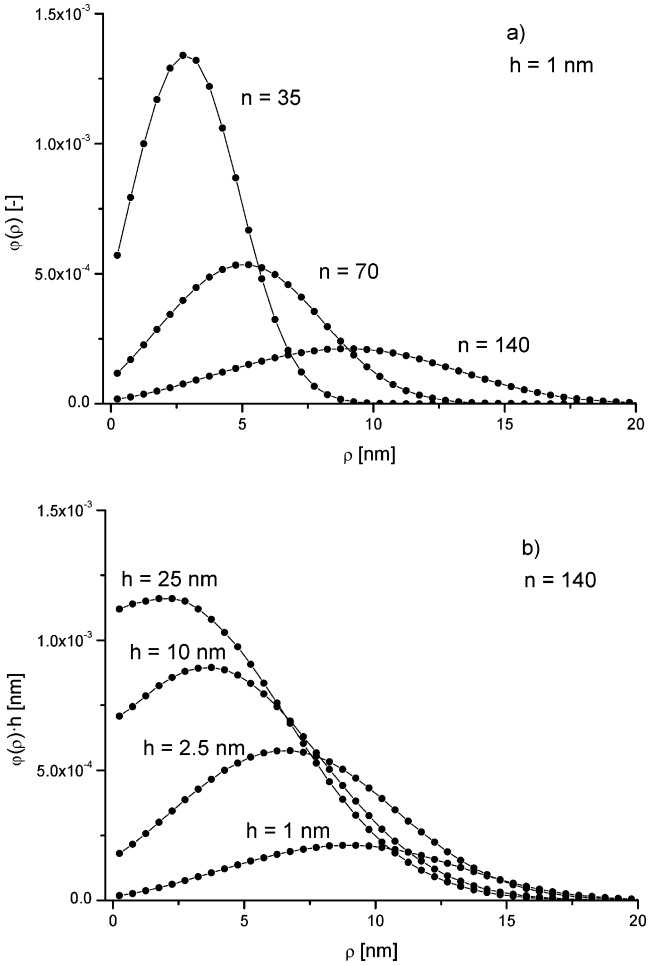

Figure 3. Radial end-segment distribution of grafted chains for (a) different degrees of polymerization (n) of the side chain at constant grafting density ($h = 1$ nm) and (b) different grafting densities (h) at constant number of monomers per side chain ($n = 140$). Calculations done for good solvent conditions ($\chi_{pol-H_2O} = 0$).

In Figure 3 we present the radial distribution function for the end monomers of the chains (volume fraction of the end segments vs distance from the grafting line ρ) for a given grafting density ($h = 1$ nm, corresponding to one grafted chain per two monomers of the backbone) and different chain lengths (Figure 3a) and for constant chain length ($n = 140$) and variable grafting densities (Figure 3b). All curves in Figure 3a fulfill the condition $h < n^{1/2}a$; i.e., the grafted chains are forced to overlap.

The distributions presented in Figure 3 demonstrate the large-scale fluctuations in the positions of the end segments of the grafted chains in the radial direction. For nonoverlapped or weakly overlapped chains (small n or/and large h), the end-segment density does not vanish in the vicinity of $\rho = 0$. This shape of the distribution is similar to that for a single grafted chain and indicates that the chain conformation is weakly perturbed by the interactions with other chains in the brush; the weak depletion zone near the origin appears because of the steric restrictions imposed for the monomers of the grafted chain by the backbone. Upon increasing the grafting density, the maximum in the end-segment distribution (characterizing the average

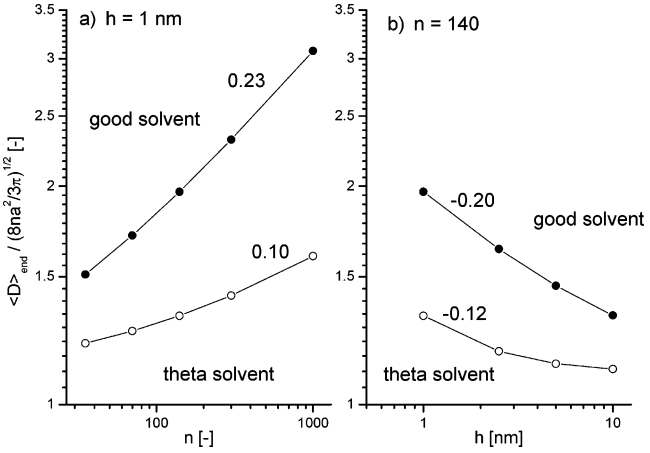

Figure 4. Average extension of grafted side chains compared to a Gaussian chain, expressed via the first moment of the end monomer distribution, reduced by $(8na^2/3\pi)^{1/2}$: (a) effect of polymerization degree of the side chain (n); (b) effect of grafting densities (h^{-1}). Calculations done for good (●, $\chi_{pol-H_2O} = 0$) and theta (○, $\chi_{pol-H_2O} = 0.5$) solvent conditions.

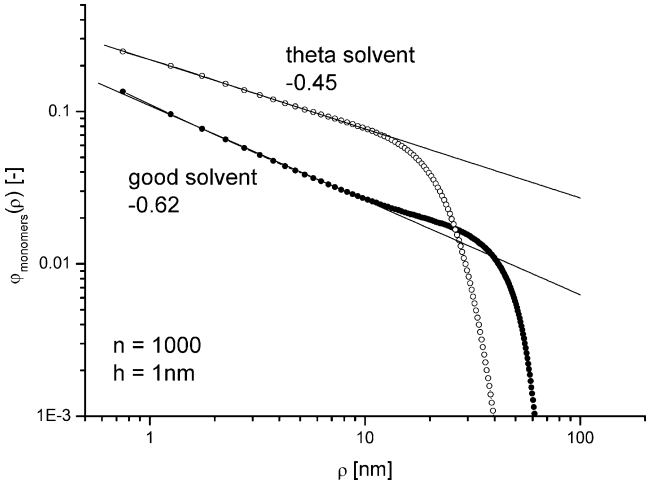

Figure 5. Radial monomer density distribution of grafted side chains. Degree of polymerization $n = 1000$; grafting density $h = 1$ nm.

end-segment position) gets displaced to larger ρ values. This indicates the progressive stretching of the chains due to the growing interchain repulsion in the brush. Simultaneously, a "dead zone", where no end monomers are located, appears in the central region of the bottle brush (at small ρ).

The first moment, $\langle D\rangle_{end}$, of the end-monomer distribution (reduced by the first moment of the Gaussian distribution, $(8na^2/3\pi)^{1/2}$) characterizes the average extension of chains in the radial direction; the corresponding log−log plots are presented in Figure 4a as a function of n for constant $h = 1$ nm and in Figure 4b as a function of h for $n = 140$. The absolute values of the ratio $\langle D\rangle_{end}/(8na^2/3\pi)^{1/2} > 1$ again indicate the extension of the chains in the bottle brush with respect to the Gaussian (unperturbed) dimensions. As expected, upon an increase in h, this ratio decreases approaching asymptotically (at large h) a constant value slightly larger than unity. Here the conformations of the grafted chains are not perturbed by interactions with other chains. However, the chain dimensions remain larger than those for a Gaussian coil due to the intramolecular repulsions and steric restrictions imposed by the backbone.

Remarkably, the curve in Figure 4b follows approximately a single-exponent power law dependence only in the range of small h, where the chains overlap considerably. The slopes of the curves in Figure 4a increase weakly but progressively as a function of n and asymptotically approach the values of the corresponding exponents predicted by eq 3.

Additional insights in the internal structure of the bottle brush is given by the radial monomer density distribution presented (in double-log coordinates) in Figure 5. The monomer density profile is a monotonically decreasing function of ρ. One can clearly distinguish between the internal region, where the monomer density decreases as a single-exponent power law (linear part in double-log coordinates), and the peripheral region near the edge of the brush, where the density profile does not obey a simple power-law dependence on ρ. The log−log slopes of the monomer density profile in the internal region are in agreement with exponents predicted by eq 5.

4.2. Bending of the Bottle Brush. Upon an increase in curvature (decrease in R), the bottle brush progressively loses its local cylindrical symmetry, as a response to bending. The effect becomes most pronounced for curvature radii comparable with the characteristic thickness of the bottle brush.

The repartition of a fraction of chains from the concave to the convex side of the brush is illustrated in Figure 6 and reflects the minimization of the free energy penalty induced by the additional crowding of chains at the concave side as a consequence of the bending of the bottle brush. The ratio between the average number of monomers (as well as end segments) localized on the convex and concave sides of the brush monotonically increases as a function of curvature.

The bending moduli have been calculated for two systems: (i) a nonconfined bottle brush in solution and (ii) a bottle brush with the main chain strongly adsorbed onto an impermeable and inert for the grafted chains flat surface. For the latter case, one mirror in the lattice system has been replaced by an impermeable plane (Figure 7).

The difference in the free energy of a brush (per unit length), $\Delta F(h,r)/hk_BT$, where $R = r^*$, between the reference ("straight") and bent configuration was computed as a function of the curvature, $1/R$, of the backbone for small ratios D/R. In our calculation scheme the reference state corresponds to the ring-shaped bottle brush with such a large curvature radius R that the conformation of the grafted chains and the free energy virtually do not depend on R. This is the case when R exceeds D by an order of magnitude. The corresponding bending modulus, κ_b/k_BT, describing induced rigidity of the bottle brush according to eq 6, was calculated from the $\Delta F(h,R)/hk_BT$ vs $1/R^2$ curves presented in Figure 8.

In Figure 9 the bending modulus is presented in log−log coordinates as a function of n for constant and high grafting density ($h = 1$ nm) and also as a function of h for the longest chains investigated. The exponents of the power law dependences of the bending modulus on n and h can be compared with the mean-field theory predictions, eq 7: The higher the degree of overlapping of the chains in the brush, the better the agreement between the SCF calculations results and the asymptotic theory predictions. Figure 10 demonstrates that the bending rigidity grows stronger (upon an increase

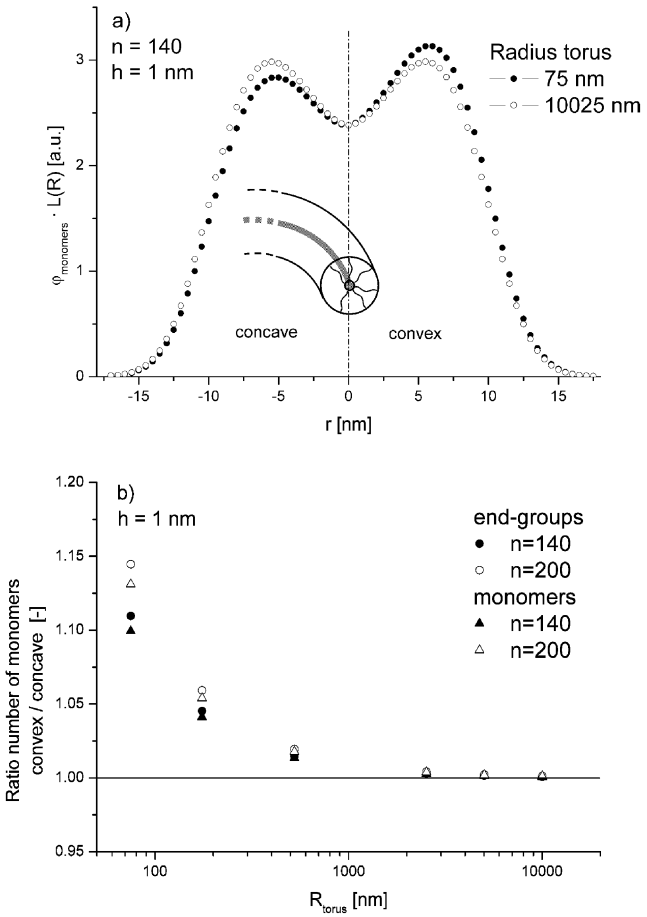

Figure 6. (a) End-segment distribution on the concave and convex side of the torus for different torus radii. (b) Ratio of the number of monomers in the convex side over the number in the concave side for different torus radii. The chain repartitioning is more pronounced for smaller radii.

Figure 7. Bent molecular bottle brush in solution (left) and adsorbed on a flat surface (right). Bending modulus increases upon adsorption due to confinement of grafted chains in a semispace.

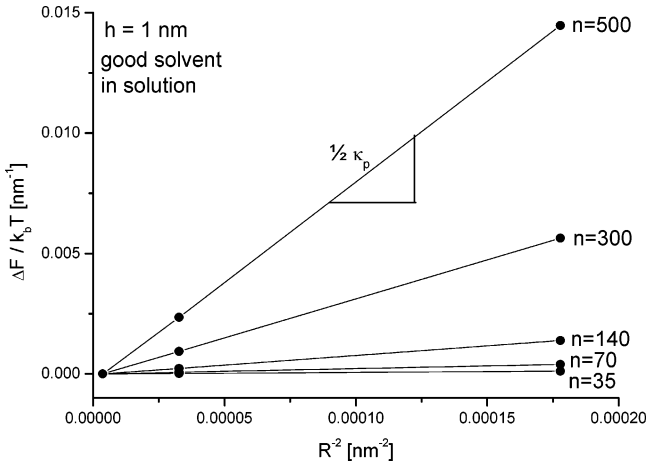

Figure 8. Change in free energy per unit length of the bottle brush upon bending. Values are displayed for different side chain lengths ($n = 35-500$) for a bottle brush in solution under good ($\chi_{pol-H_2O} = 0$) solvent conditions. As a reference state the conformation of the bottle brush with a large curvature radius ($R = 525$ nm) is chosen. The slopes of the curves correspond to half the bending modulus κ_p of the bottle brush (see eq 6).

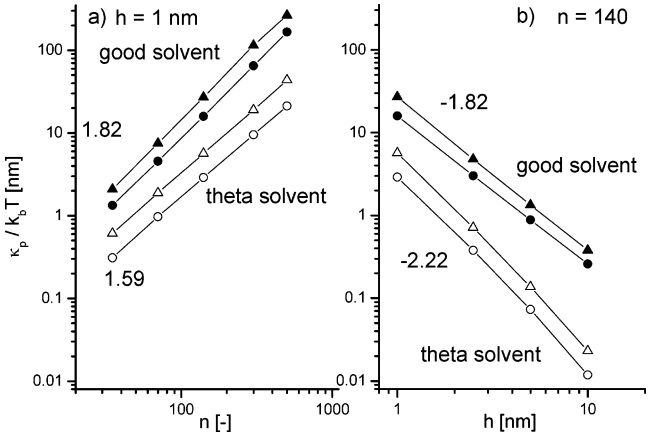

Figure 9. Bending modulus κ_p of the bottle brush in solution (circles) and adsorbed on a flat surface (triangles) for (a) different degrees of polymerization (n) of the side chain at constant grafting density ($h = 1$ nm) and (b) different grafting densities (h) at constant number of monomers in the side chain ($n = 140$). Calculations done for good (full symbols, $\chi_{pol-H_2O} = 0$) and theta (open symbols, $\chi_{pol-H_2O} = 0.5$) solvent conditions.

in n) than the characteristic thickness of the brush $\langle D \rangle_{end}$; this is again in agreement with predictions of eqs 3 and 7.

5. Discussion

The results of our SCF calculations provide quantitative insights into the conformations of grafted chains, polymer-induced bending rigidity, and large-scale conformations of molecular bottle brushes. This is significant for a better understanding of the adsorption behavior of the PLL-*g*-PEG molecular bottle brushes and the mechanical and biointeractive properties of adsorbed polymeric layers. Furthermore, the induced rigidity of the bottle brushes determines their potential ability for lyotropic ordering in solutions and in adsorbed interfacial layers.

5.1. Conformations of Grafted Chains in the Bottle Brush. As discussed above, the analytical mean-field theory provides an adequate description (in terms of power-law dependences) of conformations of the grafted chains in the asymptotic limit of their strong extension with respect to the Gaussian dimensions. This strong extension arises when the degree of overlap of grafted chains in the bottle brush is large enough, $n^{1/2}a/h \gg 1$. The overlap of the side chains is achieved by a high grafting density (small h) and/or a large degree of polymerization of the grafted chains (large n). Because the grafting density is limited by the monomer size, $h \geq a$, the asymptotic limit of strong chain overlap and corresponding strong extension is reached upon an increase in n. However, because of the cylindrical geometry of the bottle brush, the free energy of repulsive interactions per chain grows only weakly as a function of n. In the range of $10^1 \leq n \leq 10^2$, which is relevant both for experimental systems and in numerical modeling (MC, MD, or SCF-SF), the extension of chains, measured e.g. by the ratio $D/n^{1/2}a$, is not very large. This explains why the deviations between the asymptotic analytical theory predictions and more accurate (free

of approximations of strong and equal chain stretching) SCF modeling are found to be significant in this range of n, in particular with respect to the internal conformational structure of the bottle brush.

Considering Figure 5 and Figure 3, we can conclude that a bottle brush consists of two regions: (i) A central region, depleted from the end segments; in this region all the chains are stretched approximately equally (though nonuniformly), giving rise to an approximate power law radial decay of the monomer density with exponents close to those predicted by the mean-field analytical theory. (ii) A peripheral region where the end segments are distributed and the polymer density vanishes smoothly at the edge of the brush. This result is consistent with earlier theoretical predictions.[29] We emphasize that this two-region structure of the brush is well-defined only under conditions of significant overlap and extension of grafted chains (e.g., at given h for sufficiently large n), while at moderate degrees of extension these two regions are not distinguishable. The internal structure of the brush predicted from SCF calculations, with the chain ends being "allowed" to fluctuate, is dramatically different from that assumed in a simple analytical mean-field model, where the chain ends are "pinned" at the edge of the brush. However, the integral properties of the bottle brush, such as the average thickness, are well described by simple power-law dependences predicted by the approximate analytical theory, provided n is large enough.

The fact that the end-segment distribution fluctuates over a wide range within the brush is especially relevant when functional groups such as biotin are attached at the end of the side chains. These large fluctuations of the end segments can strongly decrease the availability of (e.g., biotin) binding sites for molecular recognition applications.[35]

5.2. Induced Bending Rigidity and Apparent Persistence Length. An important result of the SCF modeling is an improved quantitative insight into induced bending rigidity and large-scale conformations of the bottle brushes as a function of the molecular architectural parameters of the brush (n, h). This bending rigidity, similarly to the average thickness, is an integral property of the bottle brush. The power law dependence of the induced rigidity (bending modulus) on the architectural parameters of the brush (n, h) predicted by analytical mean-field theory (section 2) is in good agreement with our SCF calculations, thus appearing to be relatively insensitive to the details of the local conformational structure of the bottle-brush. However, the absolute values of the induced bending rigidity are determined by a delicate balance of different contributions to the free energy of the brush, depending on the cylindrically asymmetrical rearrangement of the internal structure of the brush upon bending. Because of the limited predictive abilities of the analytical theories, this balance has not been properly (quantitatively) captured before. Our SCF calculations show that, in accordance to the picture proposed in ref 11, the repartitioning of the chains from the concave to the convex side of the bent bottle brush causes a considerable reduction to the free energy penalty for the bending. Indeed, this leads to very small numerical prefactors (<0.02) in eq 7 for the induced rigidity of the bottle brush. (The scaling arguments alone used for derivation of eq 7 did not enable us to quantify these prefactors.)

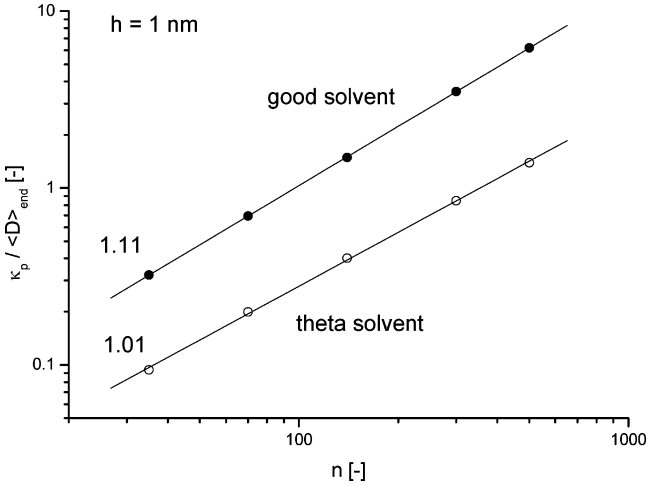

Figure 10. Ratio of induced bending rigidity (κ_p) over thickness of the brush ($\langle D\rangle_{end}$) as a function of polymerization degree of the grafted side chains (n). The ratio describes the effective segment asymmetry. Calculations done for good (●, $\chi_{pol-H_2O} = 0$) and theta (○, $\chi_{pol-H_2O} = 0.5$) solvent conditions.

As follows from the results of the SCF calculations both the induced rigidity, κ_p, and the ratio l_p/D increases as a function of D. Upon an increase in the length of grafted chains n, this ratio progressively increases. In Figure 10 the ratio l_p/D is presented as a function of n for $h = 1$ nm. The total rigidity of the bottle brush with intrinsically rigid backbone is dominated by the "bare" rigidity of the backbone, $l_{app} \approx l_{bare}$, at small n, while at large n the total rigidity is dominated by the contribution from the grafted chains, $l_{app} \approx l_p \gg D$. For PLL-*g*-PEG copolymers this situation occurs at low pH and small ionic strength in the solution, where κ_{OSF} is large. The large values of the ratio l_{app}/D, characterizing the asymmetry of the effectively rigid segment of the bottle brush, attained for large n suggest that lyotropic order may be observed in solution at sufficiently high polymer concentration.

For molecular bottle brushes with flexible, $l_{bare} \leq h$, backbones (that is the case at high pH and/or large ionic strength for PLL-*g*-PEG), the induced rigidity manifests itself in the apparent persistence length (i.e., in the effective segment asymmetry and large-scale conformational properties of the molecular bottle brush) only when it significantly exceeds the characteristic length proportional to the side chains dimensions (effective brush thickness) D. The results of our calculations prove that even for densely grafted bottle brushes this occurs only in the limit of large degrees of polymerization of the side chains (n of the order of 10^3). At smaller lengths of the grafted chains the apparent persistence length of the bottle brush scales proportionally to the dimensions of grafted chains; i.e., on the coarse-grained scale the graft-copolymer molecule can be seen as a flexible chain with an effective segment size $\sim D$.

In earlier numerical (MC) simulations[18−20] the apparent persistence length was extracted directly from the analysis of the large-scale conformational properties of molecular bottle brushes with intrinsically flexible backbones. Even though large grafting densities were chosen, the length of the grafted chains was varied over a limited range only. For those small n values, it was reported that $l_{app} \sim D$ (with an approximately constant prefactor larger than unity). As follows from results of our calculations (Figure 10), the regime $l_{app} \approx l_p \gg D$,

where the induced persistence length manifests itself in large-scale conformational properties, is reached asymptotically only for long side chains. Moreover, when the apparent persistence length is determined from large-scale structural characteristics, a large number of grafted chains in the bottle brush must be modeled. Therefore, it becomes clear that such analysis is extremely CPU-intensive when performed by MC or MD simulations.

The same problem arises in experiments. Typically only bottle brushes with relatively short grafted chains are available. Recent small-angle neutron scattering (SANS) studies[36] on partially deuterated poly(chlorovinyl ether)-*graft*-polystyrene have indicated an increase in apparent persistence length as a function of the degree of polymerization of side chains, but the influence of n on the ratio l_{app}/D was not investigated. Taking into account the degrees of polymerization of the side chains, we expect the effects of induced rigidity not to be manifested in this experiment. The determination of conformational properties of molecular brushes by SANS still remains a challenging experimental problem.

We conclude that the effect of induced bending rigidity on the large-scale conformational properties of molecular brushes in solution is of marginal importance for many experimentally relevant systems due to the relatively low degree of polymerization of grafted chains in typical copolymers.

5.3. Effects of Induced Rigidity on Adsorption Behavior. The effects of induced bending rigidity of molecular bottle brushes may become more important if the graft-copolymer is strongly adsorbed onto a solid−liquid interface as is the case for PLL-*g*-PEG, when it is adsorbed on (negatively) charged oxide surfaces due to electrostatic attraction of the (positively) charged PLL backbone (Figure 7). The induced persistence length is expected to be significantly larger in the adsorbed state than in the solution due to (i) a larger bending rigidity resulting from steric restriction imposed by the surface and confinement of the grafted chains in a semispace and (ii) a lower effective dimensionality of the adsorbed polymer. Indeed, the persistence length $l^{(2d)}$ of the wormlike chain confined in 2 dimensions is related to its bending modulus κ as $l^{(2d)} = 2\kappa/k_BT$. This persistence length characterizes in-plane thermal bending fluctuations of the wormlike chain.

In Figure 9 the bending moduli for the bottle brush whose backbone is lying (i.e., strongly adsorbed) onto an impermeable plane are presented versus the length of grafted chains, n, and versus the inverse grafting density, h. As follows from eq 7, the bending moduli should be larger than those of nonconfined chains (in solution) by the factor of 2 and $2^{4/3}$ under good and theta solvent conditions, respectively. These ratios are obtained by assuming that the bending free energy for the bottle brush with the backbone localized on the surface is equal to half of that for the free (nonconfined) brush with a twice larger grafting density. However, because of depletion of grafted chains from the proximal to the surface region, the observed increase in bending moduli is slightly weaker (1.6 ± 0.15 for good solvent, 1.9 ± 0.05 for theta solvent). Hence, the ratio l_{app}/D is larger in the adsorbed state than in solution, which may potentially result in a stronger tendency for lyotropic orientational ordering of the copolymer molecules in the adsorbed layer. This feature of the polymeric layer may be important for understanding of complex phenomena of interactions of proteins with the polymer-modified surface.

Our model assumes that there is no attractive interaction between side chains and the surface and no side chain adsorption, as it is the case, e.g., for PEG and oxide surfaces. An alternative picture arises when the adsorption is induced by attraction of side chains to the surface.[22,37] In the latter case both the backbone and the side chains are localized (confined) on the surface, and the molecular bottle brush exhibits quasi-two-dimensional behavior. In particular, because of asymmetrical distribution of the side chains with respect to the backbone, the latter acquires spontaneous curvature which leads to helical shape of the macromolecule as a whole.

In the context of the adsorption behavior and structure of adsorbed layers formed by amphiphilic copolymers, our findings imply that even under the condition of dense grafting of the side chains the graft-copolymer molecules in solution possess sufficiently large flexibility and are therefore in principle, when adsorbed on surfaces, capable of forming relatively short loops separating adsorbed sequences. This phenomenon obviously highly depends on the ratio L/l_{app}. For $L/l_{app} \gg 1$ this would then lead to an inhomogeneous structure of the adsorbed layer. In fact, it has been shown for PLL-*g*-PEG copolymers that protein resistance of the polymeric layer is lost for polymers with long PLL backbones (MW 300 kDa).[2] In the case of copolymers with a shorter backbone (MW 20 kDa), the protein-resistant properties strongly depend on the ethylene glycol (EG) monomer density on the surface (i.e., combination of grafting density of the PEG side chains, PEG MW, and adsorbed polymer mass per unit surface area). Excellent antifouling behavior is only found for high EG densities (>20 EG monomers per nm^2), stressing the importance of a brushlike conformation of the side chains to achieve protein resistance.

Acknowledgment. The authors are thankful to Professor M. Cohen Stuart (University of Wageningen, The Netherlands) for his contribution in initiating of this work and to Professor N. D. Spencer (LSST, ETH Zürich, Switzerland) for numerous useful comments on the manuscript. This work was supported by ETH Zürich (project TH-33./01-3).

References and Notes

(1) Harris, J. M. *Poly(ethylene glycol) Chemistry, Biotechnical and Biomedical Applications*; Plenum Press: New York, 1992.
(2) Pasche, S.; DePaul, S. M.; Vörös, J.; Spencer, N. D.; Textor, M. *Langmuir* **2003**, *19*, 9216−9225.
(3) Ma, Y. H.; Cao, T.; Webber, S. E. *Macromolecules* **1998**, *31*, 1773−1778.
(4) Bohrisch, J.; Eisenbach, C. D.; Jaeger, W.; Mori, H.; Müller, A. H. E.; Rehahn, M.; Schaller, C.; Traser, S.; Wittmeyer, P. In *Polyelectrolytes with Defined Molecular Architecture I*; Springer: Berlin, 2004; Vol. 165, pp 1−41.
(5) Dziezok, P.; Sheiko, S. S.; Fischer, K.; Schmidt, M.; Möller, M. *Angew. Chem., Int. Ed.* **1997**, *36*, 2812−2815.
(6) Beers, K. L.; Gaynor, S. G.; Matyjaszewski, K.; Sheiko, S. S.; Moller, M. *Macromolecules* **1998**, *31*, 9413−9415.
(7) Cheng, G. L.; Boker, A. A.; Zhang, M. F.; Krausch, G.; Müller, A. H. E. *Macromolecules* **2001**, *34*, 6883−6888.
(8) Schappacher, M.; Deffieux, A. *Macromolecules* **2000**, *33*, 7371−7377.
(9) Borner, H. G.; Beers, K.; Matyjaszewski, K.; Sheiko, S. S.; Möller, M. *Macromolecules* **2001**, *34*, 4375−4383.
(10) Sheiko, S. S.; Möller, M. *Chem. Rev.* **2001**, *101*, 4099−4123.

(11) Birshtein, T. M.; Borisov, O. V.; Zhulina, Y. B.; Khokhlov, A. R.; Yurasova, T. A. *Polym. Sci. U.S.S.R.* **1987**, *29*, 1293−1300.
(12) Borisov, O. V.; Birshtein, T. M.; Zhulina, Y. B. *Polym. Sci. U.S.S.R.* **1987**, *29*, 1552−1559.
(13) Zhulina, E. B.; Vilgis, T. A. *Macromolecules* **1995**, *28*, 1008−1015.
(14) Fredrickson, G. H. *Macromolecules* **1993**, *26*, 2825−2831.
(15) Rouault, Y.; Borisov, O. V. *Macromolecules* **1996**, *29*, 2605−2611.
(16) McCrackin, F. L.; Mazur, J. *Macromolecules* **1981**, *14*, 1214−1220.
(17) Lipson, J. E. G. *Macromolecules* **1991**, *24*, 1327−1333.
(18) Saariaho, M.; Ikkala, O.; Szleifer, I.; Erukhimovich, I.; tenBrinke, G. *J. Chem. Phys.* **1997**, *107*, 3267−3276.
(19) Saariaho, M.; Szleifer, I.; Ikkala, O.; ten Brinke, G. *Macromol. Theory Simul.* **1998**, *7*, 211−216.
(20) Subbotin, A.; Saariaho, M.; Ikkala, O.; ten Brinke, G. *Macromolecules* **2000**, *33*, 3447−3452.
(21) Khalatur, P. G.; Shirvanyanz, D. G.; Starovoitova, N. Y.; Khokhlov, A. R. *Macromol. Theory Simul.* **2000**, *9*, 141−155.
(22) Khalatur, P. G.; Khokhlov, A. R.; Prokhorova, S. A.; Sheiko, S. S.; Möller, M.; Reineker, P.; Shirvanyanz, D. G.; Starovoitova, N. *Eur. Phys. J. E* **2000**, *1*, 99−103.
(23) Connolly, R.; Bellesia, G.; Timoshenko, E. G.; Kuznetsov, Y. A.; Elli, S.; Ganazzoli, F. *Macromolecules* **2005**, *38*, 5288−5299.
(24) Birshtein, T. M.; Zhulina, E. B. *Macromol. Theory Simul.* **1997**, *6*, 1169−1176.
(25) Potemkin, II. *Eur. Phys. J. E* **2003**, *12*, 207−210.
(26) Odijk, T. *J. Polym. Sci., Polym. Phys.* **1977**, *15*, 477−483.
(27) Skolnick, J.; Fixman, M. *Macromolecules* **1977**, *10*, 944−948.
(28) Zhulina, E. B.; Borisov, O. V.; Pryamitsyn, V. A.; Birshtein, T. M. *Macromolecules* **1991**, *24*, 140−149.
(29) Semenov, A. N. *Sov. Phys. JETP* **1985**, *61*, 733−742.
(30) We remark that under good solvent conditions the exponents of the power law dependences obtained in the mean-field approximation are slightly different from those obtained in refs 11 and 12 within the scaling approximation.
(31) Daoud, M.; Cotton, J. P. *J. Phys. (Paris)* **1982**, *43*, 531−538.
(32) Zhulina, Y. B.; Birshtein, T. M. *Polym. Sci. U.S.S.R.* **1985**, *27*, 570−578.
(33) De Gennes, P. G. *Scaling Concepts in Polymer Physics*; Cornell University Press: Ithaca, NY, 1979.
(34) Landau, L. D.; Lifshitz, E. M. *Theory of Elasticity*; Butterworth-Heinemann: Oxford, 1999.
(35) Huang, N. P.; Voros, J.; De Paul, S. M.; Textor, M.; Spencer, N. D. *Langmuir* **2002**, *18*, 220−230.
(36) Lecommandoux, S.; Checot, F.; Borsali, R.; Schappacher, M.; Deffieux, A.; Brulet, A.; Cotton, J. P. *Macromolecules* **2002**, *35*, 8878−8881.
(37) Sheiko, S. S.; Prokhorova, S. A.; Beers, K. L.; Matyjaszewski, K.; Potemkin, I. I.; Khokhlov, A. R.; Möller, M. *Macromolecules* **2001**, *34*, 8354−8360.

MA050871Z